Modification of Chain Extension and Crosslinking Structures of Recycled Polyester Textile for 3D Printing Filament

Lingquan Hu[a], Jianzhong Sun[b], Meng Zhang[b], Jun Liu[b], Shouxiang Jiang[a,c,d*]

a. School of Fashion and Textiles, The Hong Kong Polytechnic University, 999077, Hong Kong, China

b. Biofuels Institute, School of the Environment and Safety Engineering, Jiangsu University, 212013, Zhenjiang, China

c. Research Institute for Intelligent Wearable Systems, The Hong Kong Polytechnic University, 999077, Hong Kong, China

d. Research Centre of Textiles for Future Fashion, The Hong Kong Polytechnic University, 999077, Hong Kong, China

* Corresponding author

Email: kinor.j@polyu.edu.hk

Abstract

The increase in amount of polyester textile waste is contributing to the severity of environmental pollution because polyester cannot be easily recycled. To reduce the limits of its recyclability, a value-added recycling approach should be explored. This work introduces an approach for recycling polyester textiles into 3D printable filaments. To increase recyclability of polyester textiles, the polyester materials are modified by ADR4468 additive. After the polyester

is 3D printed, the sample with 1.0 wt% of ADR4468 shows the highest tensile and compressive strength properties compared with 1.5 wt% and 2.0 wt%, owing to its fewer voids between the printed lines, a fish scale-like morphology that spreads out, and a higher degree of crystallization. Moreover, the mechanism of modification suggests that ADR4468 extends and crosslinks the polyester chains by ring-opening reactions of epoxy groups of ADR4468 and forms sea-island structures. The sea-island structures of bonded polyester branched cores with tangled polyester shell interface areas and unbonded polyester chain areas performed suitable rheological behaviors to recycle polyester textiles for 3D printable filaments production. The filaments can be used to replace commercially available filaments, offer a sustainable option for consumers, and impact both the polyester textile-related recycling and 3D printing industries.

Highlights

- An approach is proposed to recycle polyester textiles for 3D printing filament
- The approach uses a mechanical method to recycle polyester textiles
- Recycled polyesters were modified by ADR4468 to form core-shell structures
- Core-shell structures were separated by short polyesters(sea-island structure)
- The structures met rheological behaviors for 3D printing filament

Keywords: polyester textile; waste recycling; 3D printing filament; chain extension; crosslinking

1. Introduction

Recycling polyester textiles has become a critical item of discussion for many stakeholders

in the environmental protection field [1]. Polyester textile waste is mostly landfilled (57%) or incinerated (25%) [2]. Unfortunately, polyester textiles can only be microbially degraded at very low degradation rates by fungal and actinomycete species hydrolyzing amorphous polyesters and modifying surfaces [3-5]. The isolated bacterium needs to be stabilized and grow at 30℃ before inoculation. The bacterium can produce enzymes capable of hydrolyzing PET and the reaction intermediate, mono(2-hydroxyethyl) terephthalic acid. The enzymes PETase and MHETase are somewhat heat-labile to degrade low-crystallinity PET thin film. The environmental limitation will decrease the degradation rate in nature. The landfilling cannot degrade polyester textiles. Additionally, the incinerating of polyester textiles emits green gas and particulates, which cause air pollution, potentially posing health risks[6,7]. Low microbial degradation and air pollution increase environmental loads by landfilling and incinerating disposals of polyester textile waste. Polyester textile waste has reached its storage limit because polyester cannot be properly recycled yet it is the most popular fiber used in fabrics. Recently, chemical recycling has been explored to degrade polyester into monomers as chemicals reused for industrial synthesis. High production costs and investment disadvantage chemical recycling to dispose of polyester textile waste[8-10]. With cost reduction, glycolysis has been developed as a promising method providing profit for polyester recycling[11]. This method has been reported to recycle polyester textiles into bis(hydroxyethyl) terephthalate (BHET) monomers[12]. Then, the depolymerized monomers were polymerized and produced again into polyester pellets for applications. Depolymerization and re-polymerization cause extra chemical and energy consumption in chemical recycling from

polyesters to polyesters[13]. Meanwhile, disposal of solvents and catalysts needs to be considered to avoid secondary pollution[14]. Sustainable recycling methods are urgently needed to alternate landfilling and incineration of polyester textiles.

Mechanical recycling method can recycle polyester from polyester without depolymerization and solvents to reduce production costs and limit secondary pollution risks for applications[9,10]. Thermal and hydrolytic degradation is a major problem in reducing polyester chain length and lowering rheological properties and processability[15,16]. The degradation has been used to recycle polyester bottles into polyester fibers because fiber melt spinning needs lower viscosity than polyester for bottles. However, polyesters from textiles cannot directly be recycled by the degradation. The polyesters need to be modified by additives to improve rheological properties for applications.

Chain extender is a sort of additive that can react with hydroxyl and carboxyl groups of polyesters and extend polymer chains to improve rheological properties and processability for polyester mechanical recycling. ADR4468 has been reported as an effective chain extender to bond linear polymer chains[17-21]. Since ADR4468 contains several epoxy groups which can connect polyester chains and form branched structures, mobility of the modified polyester chains is reduced to increase the viscosity of the polyester melt[20]. The improved rheological properties allow polyester melt to effectively be processed for applications. The application of recycled polyester (recycled polyethylene terephthalate, rPET) decides the modification. To stimulate the recycling of polyester textiles, the application should be considered to add value to recycled

polyester.

Developing a value-added approach to recycling polyester textile waste is timely and important. Since 3D printing has captured commercial interest and increased market demand for printable materials, it is potentially a good option to recycle polyester textile waste. Moreover, fused deposition modeling (FDM) 3D printing is similar to mechanical recycling, which can melt and extrude thermoplastic filaments. That means the thermoplastics can be printed if they can be mechanically recycled. Recently, many sources of thermoplastic waste have been recycled for 3D printing[22-28]. However, several challenges are found in recycling polyester textile waste into 3D printable materials. Their low viscosity is designed for high-speed spinning, which during 3D printing, causes the polyester to buckle when passed through the extruder and filaments cannot be formed. In order to overcome this challenge, chain extenders can be used to increase the viscosity of polymers to an appropriate value[29]. The functional groups of the chain extenders bond the polymer chains to limit their mobility, thus decreasing the melt flowability during reprocessing. Accordingly, chain extenders might be the solution for recycling polyester textile waste into 3D printing filaments, which might practice the mechanical recycling approach to alternate landfilling and incineration of polyester textiles, increase the recycling rate, improve the sustainability of polyester textiles, reduce environmental loads, and promote carbon neutrality.

In this work, polyester textile waste is recycled into printable materials by using a polymeric chain extender ADR4468 to modify the melt flow. To investigate the optimal usage of this additive, polyester textile waste is mixed with different amounts of ADR4468 and extruded

into filaments. The filaments are 3D printed into samples for material performance tests. To investigate the mechanism of how ADR4468 contributes to realizing the recyclability of polyester textile waste, the printed samples are examined through various characterization methods, including differential scanning calorimeter (DSC), X-ray diffraction (XRD), Fourier-transform infrared spectroscopy (FTIR) analyses, rheological tests, scanning electron microscope (SEM) observations, tensile tests, and compressive tests.

2. Experimental Section

2.1 Materials

Polyester textile was purchased from Zhaoxin Xinbojin Textile Co. and used as post-consumer polyester textile waste which contained 100% polyester fibers. Joncryl ADR4468 was purchased from BASF.

2.2 Polyester textile recycling

Fig. 1 shows the recycling approach which transforms polyester textile waste into 3D printing filaments. Table 1 lists the parameters for optimal filament extrusion of polyester-based thermoplastics. Before the reprocessing commenced, the polyester textile was washed and dried at 60℃ overnight, which removed dust from the polyester fiber surface. Then, the clean textiles were hot-pressed into a paper-thin plastic board with heat-pressure equipment (ST, Lugong, China) at a temperature of 270℃ under a load of 10 MPa for 1 min. After air-cooling the plastic

board down to room temperature (20℃ to 25℃), it was grounded with 1.0 wt%, 1.5 wt%, and 2.0 wt% of ADR4468 (hereinafter rPET/ADR4468-1.0 wt%, rPET/ADR4468-1.5 wt%, and rPET/ADR4468-2.0 wt%, respectively) into powder by using a high-speed grinder (RS-FS, Royalstar, China) at 8000 rad/min for 1 min. To transform the powder into filaments, the powder was fed into a filament extruder (WSJ-12, Xinsuo, China). The extruder further mixed and melted the powder into a thermoplastic fluid. The thermoplastic fluid was then pushed out of the extruder, pulled through the die, and into the water tank and cooled in deionized water (50℃). The major axis diameter of the filaments is 1.91 mm and the minor axis diameter is 1.32 mm at the oval cross-section, which corresponds to 3D printable filament diameters of $1.75^{+0.25}_{-0.55}$ mm. In Table 1, Zones I to IV are the die, metering, compression, and feeding zones, respectively, marked on the extruder in Fig. 1. After rolling, the filaments rPET/ADR4468-1.0 wt%, rPET/ADR4468-1.5 wt%, and rPET/ADR4468-2.0 wt% were obtained for 3D printing.

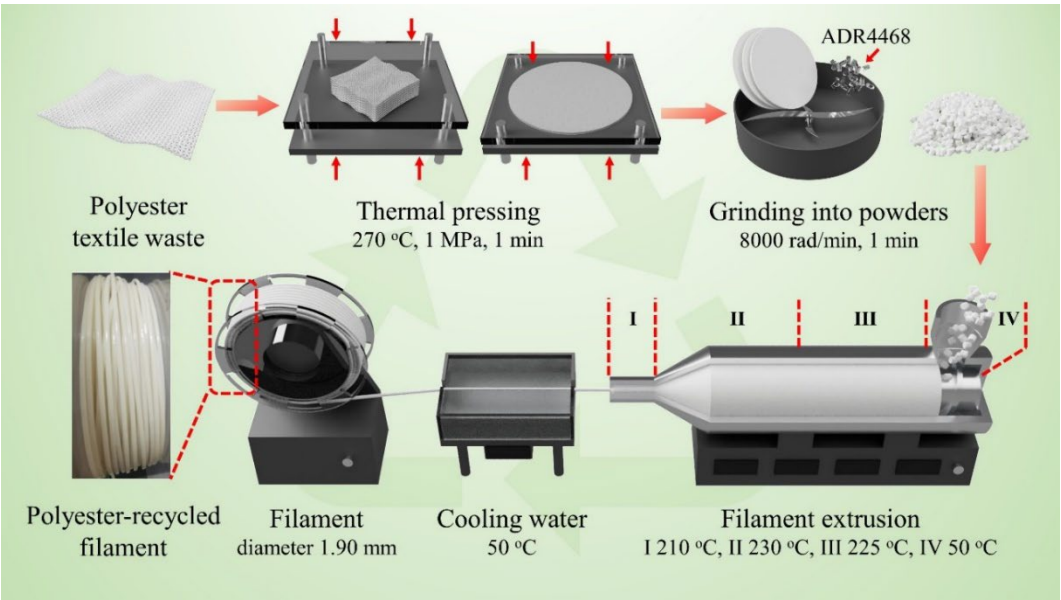

Figure 1. Polyester textile recycling for polyester-recycled filaments.

Table 1. Major parameters of rPET/ADR4468 filament extrusion

Extrusion parameter	Value
Zone I temperature	210℃
Zone II temperature	230℃
Zone III temperature	225℃
Zone IV temperature	50℃
Cooling water temperature	50℃
Screw speed	60 rad/min

Notes: Zones I, II, III and IV denote die, metering, compression, and feeding zones.

2.3 3D printing using polyester filaments

To determine the material properties, the filaments were 3D-modeled and 3D-printed into standard samples. The 3D models were designed and built with Pro/Engineer, a 3D modeling software (Pro/E 5.0, Parametric Technology Corporation Creo, USA) according to testing standards. The Pro/Engineer software exported the 3D models into STL files for the 3D printing slicer software (Cura 4.10.0, Ultimaker B.V., the Netherlands) which sliced the models into layers. However, the 3D printed parts were not entirely dense with empty space, so an infill pattern was needed. Patterned lines were used to fill the parts that were the 3D printing or nozzle extrusion path. Moreover, the slicer software sets the 3D printing parameters based on the material characteristics of the filaments. These parameters directly determine the quality and

outcome of the 3D printing, as shown in Table 2. After setting the parameters, the slicer software converted the modeled parameters into GCODE files. GCODE is a programming language that controls the 3D printer (JGMaker-A6, JG AURORA, China) to print the samples according to the sliced models. After printing, the samples were cooled down to 25℃ and removed from the print plate to reduce potential deformation of the samples.

Table 2. 3D printing parameters using Cura software.

3D printing parameter	Value
Filament material	rPET/ADR4468
Nozzle size	0.4 mm
Layer height	0.2 mm
Wall thickness	0.8 mm
Infill density	100%
Infill pattern	Lines
Printing temperature	270℃
Build plate temperature	70℃
Flow	110%
Printing speed	30 mm/s

2.4 Characterization

Several characterizations were done to investigate the effect of the weight ratio of ADR4468

on the material properties, including the crystal and chemical structures, thermal performance, morphology, rheology, and mechanical performance.

The crystal structures of the 3D printed samples were analyzed by using an XRD system (D8 ADVANCE, Bruker Co., USA) with Cu Kα as the radiation source at λ=1.54056 Å over an angular range of 10º and 60º. The chemical structures of the polyester textiles and filaments, and 3D printed samples were identified by using an FTIR spectrometer (ALPHA II, Bruker Co., USA). The thermal performance of the polyester textiles and filaments, 3D printed samples, and ADR4468 were examined by using a DSC (DSC4000, PerkinElmer, USA) at temperatures from 30℃ to 300℃ at a heating rate of 10℃/min under a nitrogen gas flow of 20 ml/min. The morphology of the cross sections of the 3D printed samples was observed under an SEM (S3400, Hitachi High-Tech Co., Japan) at 20 kV for tensile stress. The rheological performance of the textile-compressed plates and 3D printed plates was evaluated by using a rheometer (Haake MARS III, Thermo Fisher Scientific co., USA) with a plate diameter of 25 mm from 10^{-1} to 10^{2} rad·s^{-1} with dynamic frequency sweeps (ω) at 270℃ under 1% strain. The mechanical performance of the 3D printed samples was tested by examining the tension and compression (E43, MTS System Co., USA). The tensile tests were conducted in accordance with ISO 527 standard at a displacement rate of 10 mm/min. The compression tests were based on ISO 604 standard at a rate of 2 mm/min.

3 Results and discussion

3.1 Crystal structure analysis

The crystal structures of the polyester textile and rPET/ADR4468 samples were analyzed through XRD (Fig. 2). The three characteristic peaks of polyester textile and rPET/ADR4468 at 2θ values of 17.5°, 22.8°, and 25.8° correspond to the (0 1 0), (1 -1 0), and (1 0 0) crystal planes of polyethylene terephthalate (PET)[30,31]. The broad peaks and noisy XRD patterns are attributed to the semi-crystallization of the polyester chains. When the polyester chains rapidly cooled down, small crystalline regions formed during the 3D printing. The randomly distributed crystalline regions resulted in larger characteristic peaks and amplified the XRD noise level. Compared with rPET/ADR4468-1.5 wt% and rPET/ADR4468-2.0 wt%, rPET/ADR4468-1.0 wt% has the highest peak intensity at 25.8° of the (1 0 0) crystal plane. The higher intensity indicates that this sample has more crystalline regions generated. It might be attributed to high chain mobility owing to small tangle effects by short polyester chains in rPET/ADR4468-1.0 wt%. Accordingly, the decreased intensity of characterization peaks with ADR4468 content increasing suggests that there are more polyester chains tangled, extended, or crosslinked to reduce chain mobility in rPET/ADR4468-1.5 wt% and 2.0 wt%.

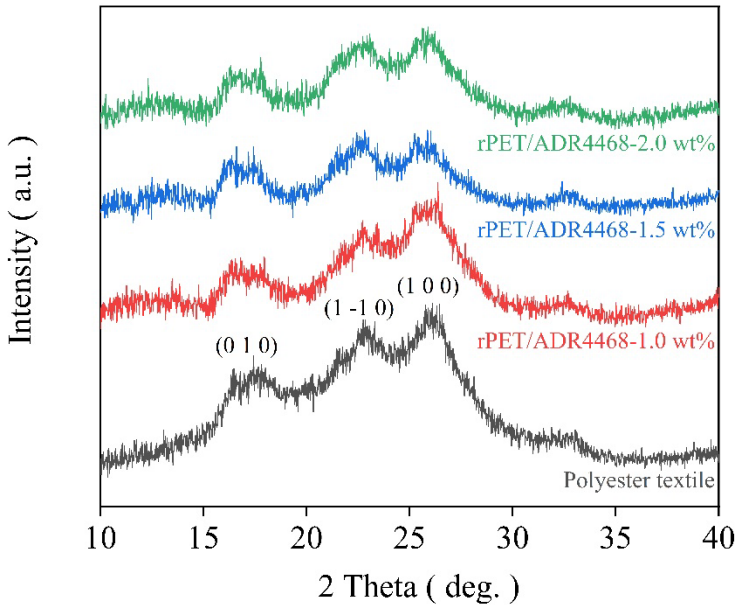

Figure 2. XRD of polyester textile, rPET/ADR4468-1.0 wt%, rPET/ADR4468-1.5 wt%, and rPET/ADR4468-2.0 wt%.

Moreover, compressive residual stress is present in rPET/ADR4468-2.0 wt%. The peaks at the (0 1 0) and (1 -1 0) planes are slightly larger towards a higher 2θ angle compared to rPET/ADR4468-1.0 wt% and 1.5 wt%. This phenomenon might be due to the compressive residual stress[32]. According to Bragg's law $2d \cdot \sin\theta = n\lambda$, the peaks that shift towards a high 2θ angle means that the spacing between the crystal planes of rPET/ADR4468-2.0 wt% (d in Bragg's law) is reduced under X-ray irradiation at a constant λ. The smaller planes suggest that the crystal regions are compressed by the compressive residual stress which cannot be released during 3D printing. The restriction of the stress release might be assigned to increases of the

tangled, extended, or crosslinked structures reducing chain mobility. Therefore, the tangle, extending, and crosslinking structures in rPET/ADR4468-2.0 wt% might induce compressive residual stress during 3D printing.

3.2 Chemical structure analysis

The chemical structures of the polyester textile, rPET/ADR4468 samples (1.0 wt%, 1.5 wt%, and 2.0 wt%), and ADR4468 were identified by using FTIR spectroscopy (Fig. 3a). The polyester textile and rPET/ADR4468 curves have PET characteristic peaks that reflect the hydroxyl end groups. Meanwhile, the ADR4468 curve shows the characteristic peaks of the epoxy groups.

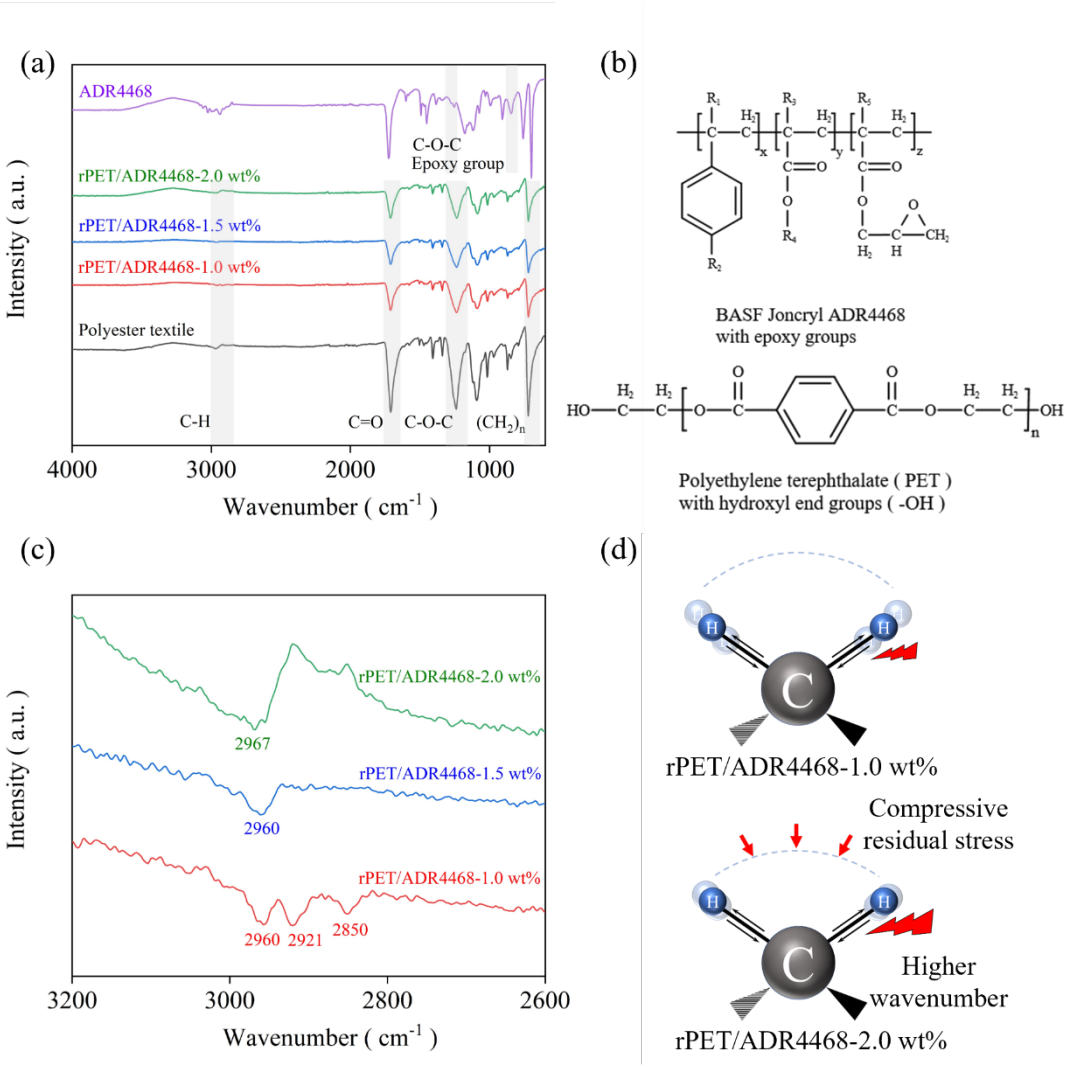

Figure 3. (a, b) FTIR of chemical structures of polyester textile, rPET/ADR4468, and ADR4468, and (c, d) compressive residual stress that shifts C-H stretching vibration of rPET/ADR4468 samples.

The polyester textile and rPET/ADR4468 samples have similar polymeric chains, which contain terephthalic acid repeat units with ethylene glycols (to form the terephthalates) and hydroxyl end groups (Fig. 3b). There are several characteristic peaks of the terephthalates. A

single peak of the C=O stretching vibration is found at 1712 cm^{-1}, which is smaller than that of the aliphatic and olefinic esters (near 1744-1739 cm^{-1})[33]. Simultaneously, a split peak of C-O-C appears at 1238 cm^{-1}, which is larger than that of the ethers (near 1225-1060 cm^{-1}). These peaks indicate that one side of C=O is connected to the C-O-C forming ester groups and the other side is attached to the C atoms of the benzene ring (benzoate esters near 1735-1720 cm^{-1}). Moreover, the attached benzoates are 1,4-disubstituted, owing to their C-H wagging vibration of the ring hydrogens near 860-800 cm^{-1}. Since none of the weak peaks of ring deformation vibration was observed, the two 1,4-substituents are both the C=O of the ester groups. These characteristic peaks show that the terephthalates produce the polyester textile and rPET/ADR4468. As diol monomers, ethylene glycols form the ester groups with the terephthalic acids specifically forming the ester groups. A single high peak of the CH_2 rocking vibration is found at 722 cm^{-1}, due to the $(CH_2)_2$ (alkane) of ethylene glycol in the crystalline state, which suggests the presence of PET crystalline regions based on the XRD analysis. Simultaneously, hydroxyl groups of the ethylene glycols are the end groups of the polyester chains. Characteristic peaks appear including the O-H stretching vibration (3600 cm^{-1}) and O-H deformation vibration of alcohol (1409 cm^{-1} and 1372 cm^{-1}). Since no characteristic peaks of carboxylic acid were observed, the hydroxyl groups are the main end groups of the polyester chains.

The ADR4468 polymer chains contain 1,4-disubstituted benzene rings, ester groups, epoxy groups, and long-chain alkyl groups (Fig. 3b). The R_1, R_2, R_3, R_4, and R_5 might be H, CH_3 or a long-chain alkyl group[34]. Since characteristic peaks of the 1,4-disubstituted benzene ring were

observed, including C-C stretching vibration and C-H bending deformation, the R_2 could be the alkyl group. A single high peak of the C=O stretching vibration (1724 cm^{-1}) and a split peak of the C-O-C stretching vibration (1180 cm^{-1}) appear, which suggests that ester groups are present and their C=O is attached to the C atoms of the alkyl groups. The two characteristic peaks of the epoxy groups (1256 cm^{-1} and 843 cm^{-1}) point to the presence of epoxy groups in the side chains. Meanwhile, some of the epoxy groups are ring-opened and produce diols (3600 cm^{-1} and 1384 cm^{-1}). To improve the elasticity, ADR4468 is added because this additive contains long-chain alkyl groups and the CH_2 rocking vibration of long-chain alkyl groups with a large sharp peak appears at a low wavenumber (699 cm^{-1}). This low wavenumber suggests that the polymer chain contains many long-chain alkyl groups in the branched chains. Based on the epoxy groups and long-chain alkyl branches, ADR4468 could reduce viscosity and improve elasticity of tangled, extended, and crosslinked polyester chains in rPET/ADR4468.

Additionally, the compressive residual stress shifts the C-H stretching vibration peak to a high wavenumber as shown by the rPET/ADR4468-2.0 wt% curve. Fig. 3c shows that the C-H stretching vibration peak integrates the split peaks (2960 cm^{-1}, 2921 cm^{-1}, and 2850 cm^{-1} in rPET/ADR4468-1.0 wt%) into a single peak (2960 cm^{-1} in rPET/ADR4468-1.5 wt%) and then shifts to high wavenumber (2967 cm^{-1} in rPET/ADR4468-2.0 wt%). According to the Planck relation $E = hc\tilde{\nu}$, when the peak shifts to a higher wavenumber $\tilde{\nu}$, the C-H bonds absorb more energy E for their stretching vibration. The vibration is restricted by local groups and its space is reduced for high activation energy. This phenomenon might be attributed to the compressive

residual stress. The residual stress compresses and reduces free space in the crystalline and amorphous regions. With the amount of free space reducing, the residual stress further restricts the C-H stretching vibration for high activation energy and shifts the peak to a high wavenumber, corresponding to the crystalline plane distance decreasing in XRD results.

3.3 Thermal performance

To investigate how ADR4468 affects polyester chain mobility, the thermal performance of the polyester textile, rPET/ADR4468 samples, and ADR4468 was examined by using DSC (Fig. 4a). The initial DSC heat curves show the effects of ADR4468 on the recycling of the polyester material through reaction temperature of ADR4468 and cold crystallization temperature (T_{cc}) and melt temperature (T_m) of the rPET/ADR4468 (Table 3).

Table 3. Thermal analysis of polyester textile, rPET/ADR4468, and ADR4468

Sample	T_g (°C)	T_{cc} (°C)	ΔH_{cc} (J/g)	T_m (°C)	ΔH_m (J/g)
Polyester textile	72.5	-	-	256.4	60.5
rPET/ADR-1.0 wt%	72.3	119.6	-21.8	259.0	50.8
rPET/ADR-1.5 wt%	72.8	115.6	-4.7	256.9	41.4
rPET/ADR-2.0 wt%	72.3	117.8	-13.0	256.7	52.1
ADR4468	-	-	-	68.7	11.9

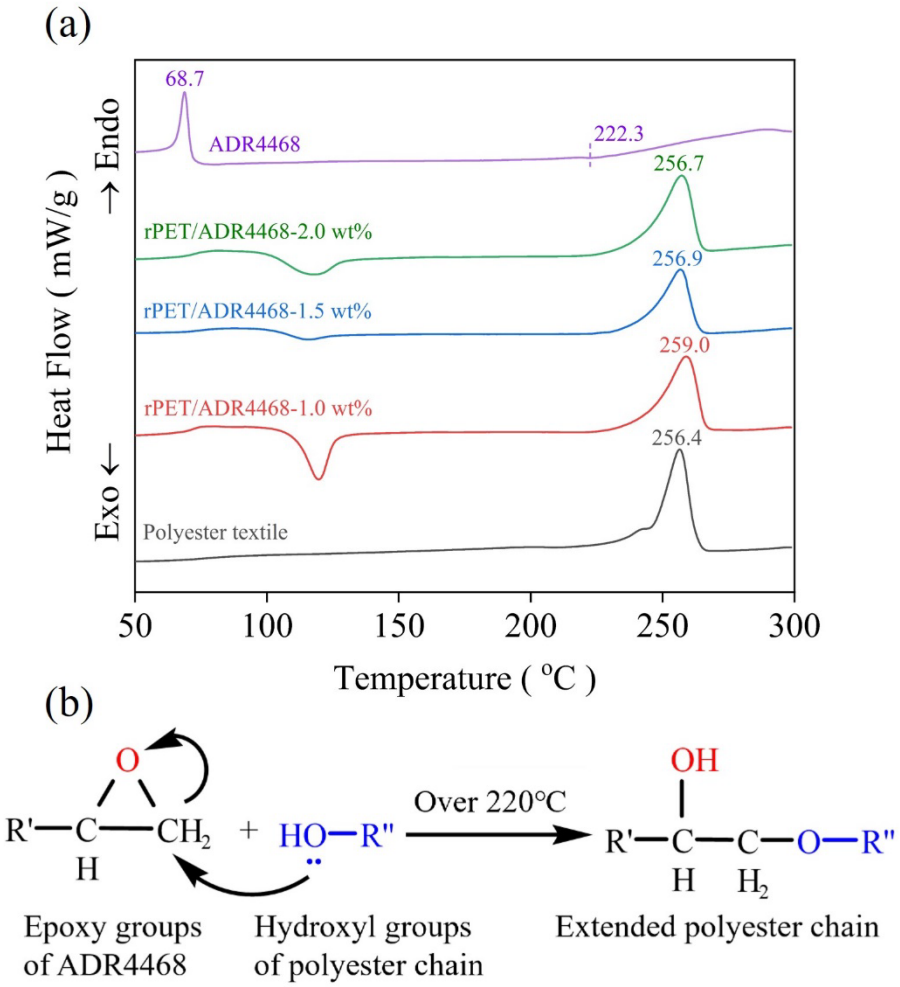

Figure 4. (a) Initial DSC heat curves of polyester textile, rPET/ADR4468-1.0 wt%, rPET/ADR4468-1.5 wt%, rPET/ADR4468-2.0 wt%, and ADR4468, and (b) Oxirane ring opening via nucleophilic addition reaction in rPET/ADR4468 filament extrusion

The endothermic broad peak of ADR4468 (from about 222.3℃ to 290.6℃, Fig. 4a) indicates that the epoxy groups of ADR4468 are activated and reacted during the extrusion (Zones II and III have a temperature over 225℃). The opened epoxy groups react with the hydroxyl end groups (-OH) of the polyester chains based on oxirane ring-opening via a

nucleophilic addition reaction in an epoxide system (Fig. 4b)[35]. Since no free acid is available to protonate the oxygen of the epoxy groups before the ring opened, the oxygen of -OH group which acts as a nucleophile would attack the less inhibited epoxide C atom[36]. After chain extension, the polyester chain is linked with the less inhibited epoxide C atom of ADR4468, and the hydroxyl group forms connections with another C atom of the epoxy group. Since ADR4468 contains two or more two epoxy groups, the polyester chains would be extended and crosslinked after the oxirane ring-opening reaction[37]. The oxirane ring-opening reaction of the epoxy groups means that ADR4468 could extend and crosslink with the polyester chains during filament extrusion. The increased generation of the extended and crosslinked structures reduced the area of T_{cc} and T_m peaks related to the crystallization of the recycled polyesters. The intensity of the T_{cc} and T_m peaks of rPET/ADR4468-1.5 wt% and 2.0 wt% decreases compared with rPET/ADR4468-1.0 wt%. The higher T_{cc} peak of rPET/ADR4468-1.0 wt% means that the polymer chains tend to crystallize due to the high chain mobility. The high chain mobility allows the chains to move fast and cold-crystallize rapidly during heating. Meanwhile, the higher peak and area of T_m indicates that rPET/ADR4468-1.0 wt% has more crystalline regions than rPET/ADR4468-1.5 wt% and 2.0 wt%, which corresponds to their higher intensity and area of crystal planes in the XRD results. Accordingly, the content increase of ADR4468 would increase the amount of extended and crosslinked structures in rPET/ADR4468 to reduce the mobility of the polyester chains with the area decreasing of T_{cc} and T_m peaks.

Remarkably, a downward trend of T_m was observed, from 259.0℃ for rPET/ADR4468-1.0

wt% to 256.9℃ for rPET/ADR4468-1.5 wt% and 256.7℃ for rPET/ADR4468-2.0 wt%. This downward trend demonstrates that there might be residual stress in rPET/ADR4468-1.5 wt% and rPET/ADR4468-2.0 wt%. Since the residual stress declined before the crystalline regions melted, the stress decline would cause the chains to unfold earlier than their melting threshold and reduce the T_m with increase in residual stress. The reduced T_m suggests that the residual stress increases with increased amount of ADR4468, which corresponds to the blue-shifting of the C-H stretching vibration in the FTIR results.

3.4 Rheological properties

The rheological properties of polyester textile, rPET/ADR4468-1.0 wt%, rPET/ADR4468-1.5 wt%, and rPET/ADR4468-2.0 wt% were measured by using dynamic rheological tests including complex viscosity, storage modulus G', and loss modulus G'' (Fig. 5) to investigate ADR4468 contents effect on polyester chains and compressive residual stress.

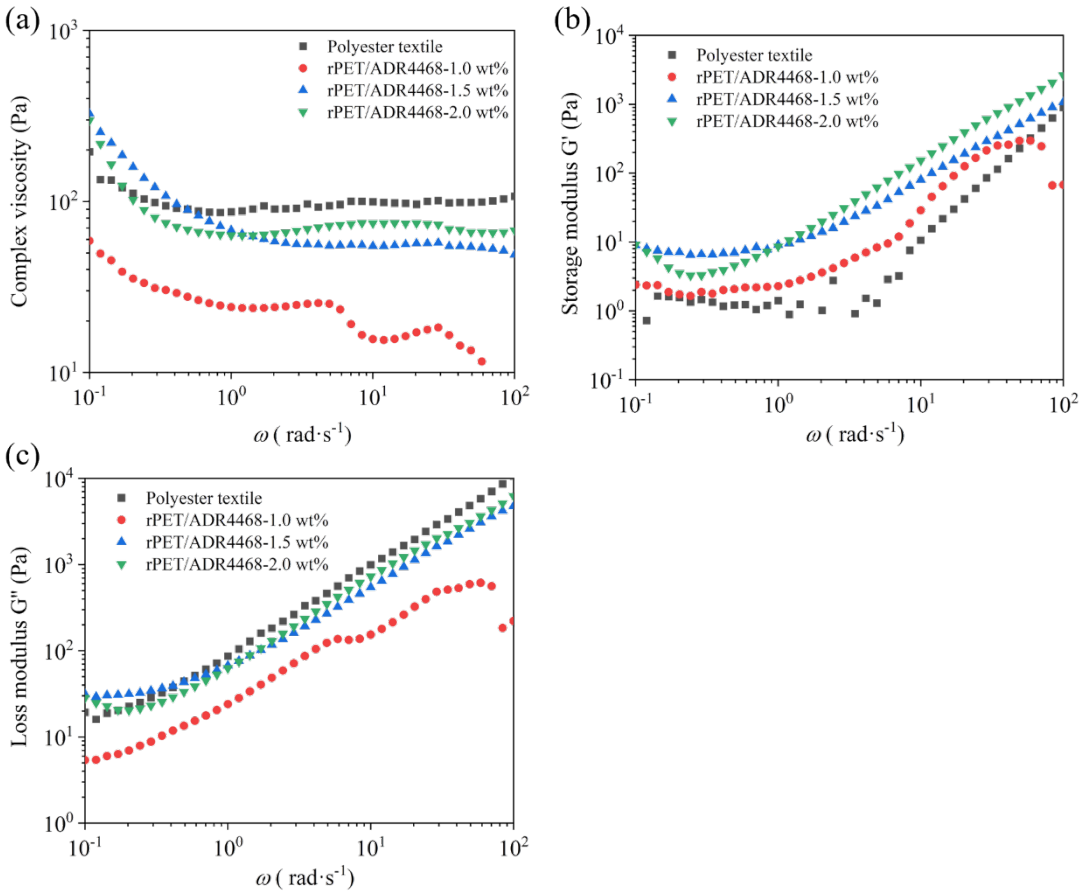

Figure 5. (a) Complex viscosity-ω, (b) storage modulus G'-ω, and (c) loss modulus G''-ω curves of polyester textile, and rPET/ADR4468-1.0 wt%, 1.5 wt%, and 2.0 wt%.

The complex viscosity measures the total resistance to flow with isothermal measurements of the frequency (ω) of shearing. Fig. 5a shows that the complex viscosity of the polyester textile and the rPET/ADR4468 samples almost decreases with increases in ω due to the shear thinning characteristics of the pseudoplastic behavior of the polyester textile and rPET/ADR4468. At the beginning of ω at 10^{-1}, the complex viscosity of rPET/ADR4468-1.5 wt% and rPET/ADR4468-2.0 wt% is higher than that of the polyester textile, owing to the existence of crosslinked

structures. The crosslinked structures connect the polymer chains into networks, which inhibit the mobility of the polymer chain and increase the complex viscosity at the beginning of their flow. In the regions with a low ω value (10^{-1} to 10^{0}), the complex viscosity of the rPET/ADR4468 samples is greatly decreased, and their rate of decrease increases with more ADR4468. This steep reduction in the complex viscosity might be attributed to the relaxation of the compressive residual stress, which would relax and deform the polymer chains, thus causing further extension of the polymer chains under the shearing stress. This further extension enhances the material response and reduces the mechanical resistance (complex viscosity) to the shearing stress. Due to the high compressive residual stress, the complex viscosity of rPET/ADR4468-2.0 wt% is further reduced to less than 1.5 wt% in the region with low ω values. In other words, the rPET/ADR4468-2.0 wt% sample exhibits a higher flowability than the rPET/ADR4468-1.5 wt% under a low shearing stress (region with low ω values). In the regions with a high ω values (10^{0} to 10^{2}), all the rPET/ADR4468 samples have a lower complex viscosity than the polyester textile. Moreover, the rPET/ADR4468-1.0 wt% sample exhibited the lowest complex viscosity with a fluctuating trend of decrease. On the other hand, the complex viscosity of rPET/ADR4468-2.0 wt% showed a slight upward trend from 10^{0} to 10^{1} and then declined. Due to the slight upward trend, the complex viscosity of rPET/ADR4468-2.0 wt% is higher than that of rPET4468-1.5 wt%. This phenomenon is attributed to the increase in the resistance of the long-chain alkyl groups after the relaxation of the compressive residual stress. The extended chains are tangled up with the neighboring chains which resist mobility under

shearing stress, thus increasing the complex viscosity of rPET/ADR4468-2.0 wt%.

The storage modulus G' represents the elasticity of the visco-elastic polymer melts. Fig. 5b shows that the storage modulus G' of the polyester textile and rPET/ADR4468 samples almost increases with higher ω values, except for the trough of rPET/ADR4468-2.0 wt% in the region with low ω values. The trough and plateau point to the presence and relaxation of compressive residual stress, respectively[38]. The latter induces extra strain and reduces the G', which corresponds to the dip at the beginning of the complex viscosity-ω curves. In the region with high ω values, the G' increases with increasing ω values due to the slow material response, thus exhibiting a solid-like mechanical performance with high rigidity. Remarkably, the G' of all of the rPET/ADR4468 samples is higher than that of the polyester textiles. Meanwhile, the G' of the polyester textile shows an upward trend with more ADR4468, except for the region with lower ω values caused by the residual stress relaxation of rPET/ADR4468-2.0 wt%. These increases in the G' suggest that ADR4468 enhances the melt elasticity of PET which affects the filament extrusion to reduce the melt dropping behavior. At the end of the extrusion (Zone IV in Fig. 1), the rPET/ADR4468 sample flowed through the narrow extrusion nozzle when it absorbed the compressive energy which converted the sample into melt and increased its elasticity. Before the sample increased in elasticity, it had to be cooled down to prevent the gravity-induced melt dropping. Due to higher elasticity, the rPET/ADR4468 samples were successfully extruded and shaped into 3D printable filaments.

The loss modulus G'' demonstrates the viscosity of visco-elastic polymer melts. Similar to

the G’ trends, the G’’ of the polyester textile and rPET/ADR4468 samples showed a slight upward trend with higher ω values (Fig. 5c), except for the trough of rPET/ADR4468-2.0 wt% in the region with low ω values. The trough could be attributed to the relaxation of the residual stress, which induces extra strain and material response that reduces the viscosity. In the regions with higher ω values, the G’’ of the rPET/ADR4468 samples is lower than that of the polyester textile, which shows that the long-chains in the polyester respond slowly to the shearing stress due to the tangled long-chains which restrict their mobility. The low viscosity means that the polymer chains of rPET/ADR4468 samples might be shorter than those of the polyester textile, although ADR4468 extends the chains. The shorter chains of rPET/ADR4468-1.0 wt% might affect filament extrusion and effectively prevent the relaxation of the compressive residual stress after 3D printing.

3.5 Morphology observations of 3D printed samples

The fractured sections of the rPET/ADR4468 tensile samples show the fracturing mechanism and quality of the 3D printing. The morphology of the samples was analyzed by using an SEM (Fig. 6). Fig. 6a shows the continuous fractures in a section of rPET/ADR4468-1.0 wt%. The continuous fractures indicate that the printed polymer is very much fused into printed lines without voids (implies high 3D printing quality), which means that rPET/ADR4468-1.0 wt% offers a high mechanical performance. To explore the enhancement mechanism from the use of the material, Fig. 6d shows a rough morphology that is fish scale-like

in the fractured section of rPET/ADR4468-1.0 wt%. The fish-scales are produced and propagate during tensile fracturing which suggests that the material is irreversibly deformed and begins to yield when tension leads to the breaking point of the sample. The slight yielding uses more energy and improves the tensile performance.

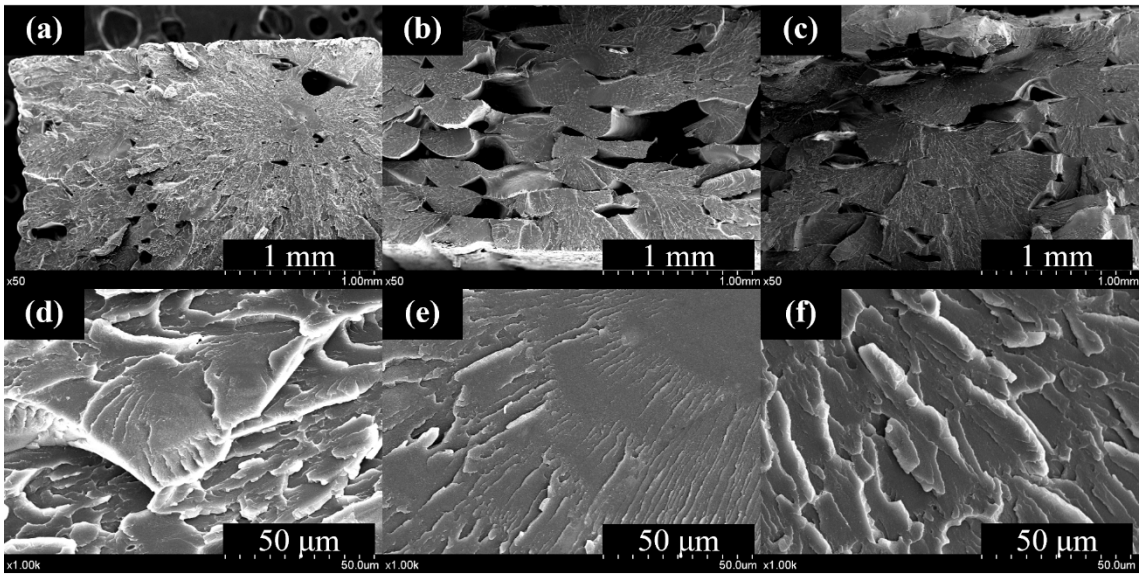

rPET/ADR4468-1.0 wt% rPET/ADR4468-1.5 wt% rPET/ADR4468-2.0 wt%

Figure 6. Fractured surface SEM image of 3D printed tensile test samples: (a,d) rPET/ADR4468-1.0 wt%, (b, e) rPET/ADR4468-1.5 wt%, and (c,f) rPET/ADR4468-2.0 wt%.

With increased amounts of ADR4468, the fractured section of rPET/ADR4468-1.5 wt% shows obvious voids between the printed lines, especially at the connecting areas (overlapping zone) between the 3D printed wall and infill (Fig. 6b). The increasing number of voids could be attributed to the high complex viscosity (Fig. 5a) of rPET/ADR4468-1.5 wt% which reduces the flow of the melt when pushed through the printing nozzle. The low flow of the melt reduces the

bond of the materials and produces the voids. Tensile stress is concentrated in the voids and fractures are initiated. Upon further observing the surface of rPET/ADR4468-1.5 wt% (Fig. 6e), a smaller fish-scale-like morphology appears and expands to the edge of the lines, which indicates that the voids inhibit the expansion of the morphology through energy absorption of the tension. Accordingly, the increasing number of voids greatly deteriorates the mechanical performance of rPET/ADR4468-1.5 wt%.

When the amount of ADR4468 was increased to 2.0 wt%, the printed lines merged again, and the number of voids was reduced, which means low complex viscosity in the region with low ω values. The low complex viscosity of rPET/ADR4468-2.0 wt% increased the flow of the melt and allowed the melt to fuse with the printed lines. Moreover, this phenomenon suggests that the shearing strength obtained through 3D printing might be similar to that at the regions of low ω values (10^{-1} to 10^{0} rad·s^{-1}) in the rheological test. This means that the compressive residual stress might be generated by compression of the melt at the nozzle (substantial shrinking from 2.0 mm to 0.4 mm) and release of the stress after extrusion of the melt through the nozzle, which increases the flow of the melt and reduce the voids on rPET/ADR4468-2.0 wt%. With fewer voids, the fish-scale morphology increases and expands on the fractured surface (Fig. 6f), at a scale in between that of the rPET/ADR4468-1.0 wt% and rPET/ADR4468-1.5 wt% samples. Therefore, the release of the stress increases the melt flow to reduce voids and enhance the mechanical performance of rPET/ADR4468-2.0 wt%.

3.6 Mechanical performance analysis

To evaluate enhancement of ADR4468 in recycled polyester materials for 3D printing application, tensile and compressive properties, testing was done in accordance with ISO 527-2/5A/10 and ISO 604/B/2, respectively. Fig. 7a shows the tensile properties with tensile strength, fracture elongation, and Young's modulus of rPET/ADR4468-1.0 wt%, rPET/ADR4468-1.5 wt%, and rPET/ADR4468-2.0 wt%. Meanwhile, Fig. 7b shows the compressive properties with compressive strength, fracture elongation, and Young's modulus.

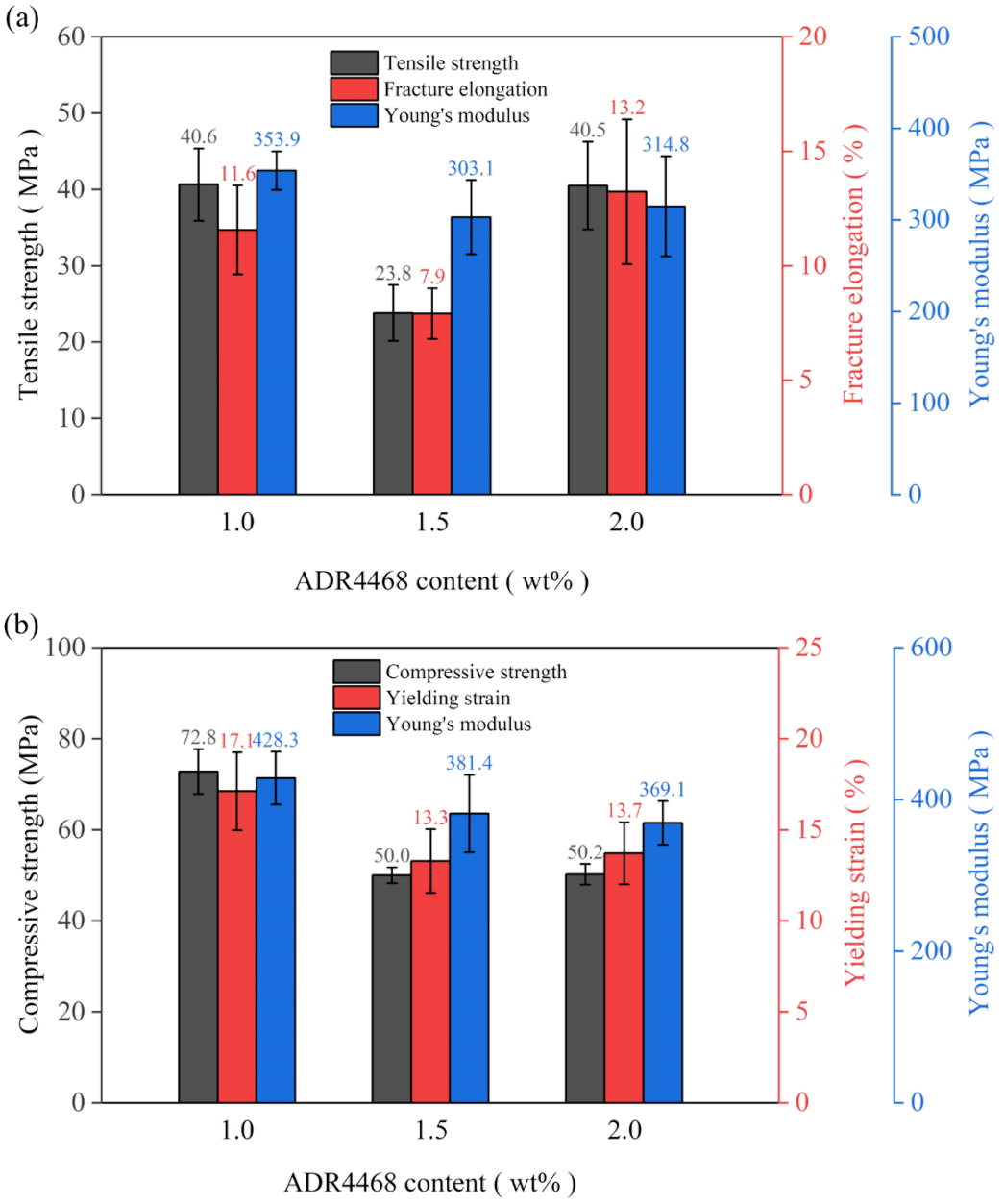

Figure 7. (a) Tensile and (b) compressive properties of rPET/ADR4468-1.0 wt%, rPET/ADR4468-1.5 wt%, and rPET/ADR4468-2.0 wt%.

rPET/ADR4468-1.0 wt% has the highest tensile (tensile strength of 40.6 MPa and Young's modulus of 353.9 MPa) and compressive (compressive strength of 72.8 MPa, fracture strain of

17.1%, and Young's modulus of 428.3 MPa) properties, which correspond to the SEM analysis that the continuous and expanded fish-scale morphology of the fractured sections enhances the mechanical performance of the samples. Since the melt of the rPET/ADR4468-1.0 wt% sample flows with ease (low complex viscosity), the melt could fill the printed area and merge with the printed lines to form a continuous section of fractures. Under tension, the continuous section of fractures allows the fish-scales to expand. The fish-scale morphology exemplifies the increase in polymer yield. During the straining, the polymer chains exhibit slight flexibility, owing to the chain extension induced by ADR4468 with flexible long-chain alkyl branches. The chains non-reversibly deform to produce the fish-scales which impart toughness, thus absorbing tensile energy. The tensile energy could also be used through the propagation of the fractures in the amorphous regions to enhance mechanical performance. According to the high intensity of the characteristic peak at 25.8° of the PET (1 0 0) crystal plane (XRD results) and endothermic peak (melting) at ~259.0°C (DSC results), the rPET/ADR4468-1.0 wt% contains many crystalline regions that are connected to the amorphous regions[39]. These crystalline regions resist the propagation of the fractures with less strain and bypass the extended propagation path of the fractures in the amorphous region to increase the energy absorption, thus increasing the mechanical strength and Young's modulus[40]. Thus, the propagation of the fractures in the amorphous regions and the slight surface toughness (fish-scales) improve the tensile properties of rPET/ADR4468-1.0 wt%.

Unfortunately, with increased ADR4468 content, rPET/ADR4468-1.5 wt% has a poor

mechanical performance in terms of the tension and compression due to a high complex viscosity and poor crystallization. The high complex viscosity reduces the polymer melt in the printed areas and produces obvious voids between the printed lines. Fewer materials in the cross-section of 3D printed samples directly deteriorate the mechanical performance. The generated voids lead to accumulation of stress and limit the spread of the fish-scales (material yielding), thus reducing energy absorption. Moreover, due to the low intensity of the crystal peaks (XRD results) and melting peak (DSC results), poor crystallization reduces and shrinks the crystalline regions, which deteriorate the resistance to fracturing, thus further reducing energy absorption. Therefore, high complex viscosity and poor crystallization erode the mechanical performance of rPET/ADR4468-1.5 wt%.

rPET/ADR4468-2.0 wt% exhibits high tensile strength (40.5 MPa) and low compressive strength (50.2 MPa), with enhanced mechanical performance owing to the compressive residual stress. According to the G' plateau in the region with lower ω values (Fig. 5b) and shifts of the C-H stretching vibration peak (red color) (Fig. 3c), compressive residual stress is found in rPET/ADR4468-2.0 wt%[32,38,41-44]. The residual stress offsets the tensile forces and gradually relaxes when the tensile stress causes the 3D printed samples to stretch. With increasing tensile stress, the polymer chains are even more elongated, thus resisting the tensile stress. When the tensile stress reaches the limitation for the deformation of the polymer chains, the chains are broken, fractures propagate, and the samples are damaged. Although the rPET/ADR4468-2.0 wt% samples contain voids, their tensile strength returns and increases with high strain due to the

compressive residual stress. At the same time, this phenomenon lends support to the fact that the compressive residual stress decreases the compressive strength with less strain. Therefore, the compressive residual stress enhances the tensile properties and deteriorates the compressive properties of rPET/ADR4468-2.0 wt%.

3.7 Modification of recycled polyester by ADR4468

3.7.1 Sea-island structure generation

Extending and crosslinking structures of ADR4468 and recycled polyester were formed by epoxy groups of the ADR4468 activation and bonding via open rings reacting with -OH end groups of the polyester chains (Fig. 4b), which improved rheological performance of the recycled polyester for producing 3D printing filament. Since there were more than two epoxy groups on ADR4468 side chains, one ADR4468 chain would connect with more than two polyester chains and grow branched structures from the main chain of ADR4468 to generate elastic cores of ADR4468-extended and crosslinked polyester chains (Fig. 8). The branched structures would tangle with unbonded polyester chains to reduce their motivation and hinder their crystallization, forming metastable elastic shells of core-tangled polyester. The elastic core-shell structures might be separated as island areas by short polyester chain areas as a sea area when a small amount of ADR4468 was blended. From extending and crosslinking reactions of ADR4468, the sea-island structures were generated by bonded polyester branched cores with tangled polyester shell interface areas and unbonded polyester chain areas in rPET/ADR4468.

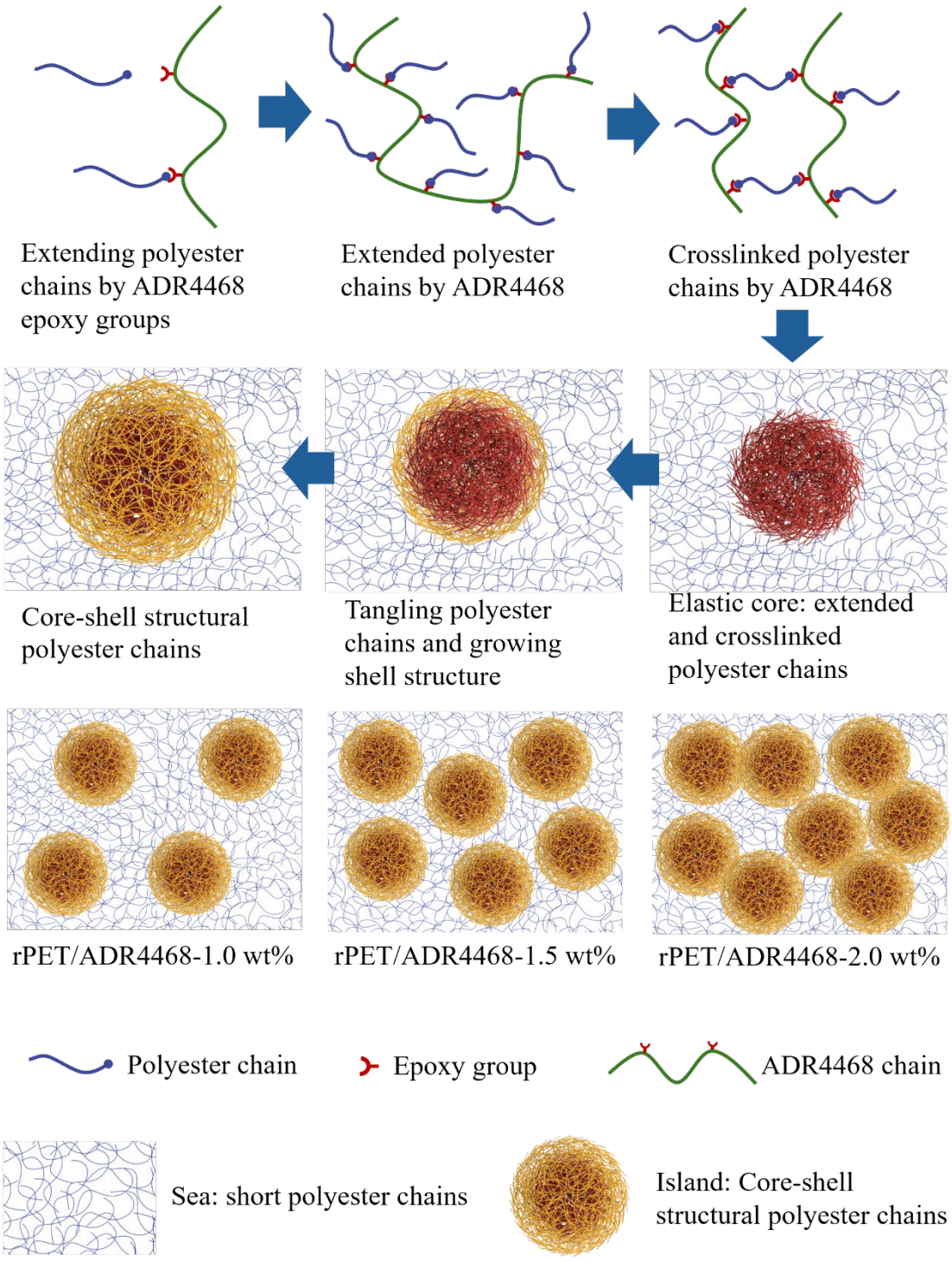

Figure 8. ADR4468 modification of recycled polyesters assembled sea-island structures of rPET/ADR4468-1.0 wt%, 1.5 wt%, and 2.0 wt% by sea area of short polyester chains and island

areas of extended and crosslinked polyester chains cores with tangled polyester chains shells.

3.7.2 Sea-island structure improving melt elasticity and 3D printing performance

The sea-island structure increased the melt elasticity of rPET/ADR4468 by its elastic core structural polyester chains extended and crosslinked by ADR4468. The bonded polyester chains formed random coils due to the restricted mobility hindering their crystallization. The random coils could deform under melt pressure to store elastic energy, characterized as melt elasticity improvement. When the rPET/AD4468 melts through narrowing nozzles of filament extruder and 3D printer, the elastic island areas would increase elastic potential energy under compression stress. The sea area of short polyester chains would lubricate and relax the compression stress of island areas to perform a low viscosity with low elasticity, which causes melt dropping and difficulty in forming filaments during filament extrusion. With ADR4468 content increasing to 1.0 wt%, the polyester sea structure would still lubricate the island structures but could not extremely relax their compressive stress to behave a low viscosity with high elasticity in rPET/ADR4468-1.0 wt% (Fig. 5). The elastic island areas would be generated enough to perform melt elasticity and keep the melt shapes before cooling down for the continuous filament extrusion. As the content reaches 1.5 wt%, the elastic areas might start to merge and separate the polyester sea structure, failing the lubrication. The rPET/ADR4468-1.5 wt% melt performed high viscosity and high elasticity, which could be extruded into filaments but not fuse printing areas to generate voids in 3D printed products (Fig. 6b). When the ADR4468 content increased

to 2.0 wt%, the elastic island structure might merge and form an elastic net structure. The elastic net structure would further increase melt viscosity and elasticity to store compressive stress at the nozzle and then might immediately release the stress to cause extrusion swell at the end of the nozzle. The extrusion swell of rPET/ADR4468-2.0 wt% allowed the melt to fuse printing area sufficiently with fewer voids in 3D printed products. Since the release of compressive stress was insufficient before the melt cooled down, the compressive stress would remain in the frozen solid rPET/ADR4468-2.0 wt% as compressive residual stress. The residual stress enhanced the tensile properties of rPET/ADR4468-2.0 wt%. As the ADR4468 content over 2.0 w%, the melt fracture happened, owing to the over-high melt viscosity and elasticity by over-thin tangled polyester interface areas and the crosslinking between the branched structures in the net structure. Therefore, the sea-island structures of bonded polyester branched cores with tangled polyester shell interface areas and unbonded polyester chain areas of rPET/ADR4468 performed suitable rheological behaviors to recycle polyester textiles for 3D printable filaments production.

4 Conclusion

To increase the recycling rate of polyester textiles, this study has introduced a value-added approach to recycling polyester textiles by blending ADR4468 into 3D printable materials. The recycled polyester rPET/ADR4468-1.0 wt% has optimal tensile and compressive properties. Its high mechanical performance could be attributed to fewer voids, extension of a fish-scale morphology, and good crystallization. Remarkably, compressive residual stress is found in the

rPET/ADR4468-2.0 wt% sample, which accounts for its high tensile properties with low compressive properties. The residual stress reduces the complex viscosity in the area with low ω values (10^{-1} to 10^{0}), which allows more polymer melt to flow through the nozzle of the 3D printer to fill the printed area, thus reducing the number of voids and improving the mechanical performance. Moreover, the mechanism of ADR4468 additive modification suggests that the additive extends and crosslinks the polyester chains by the ring-opening reaction of the epoxy groups of ADR4468 and forms sea-island structures of rPET/ADR4468. The sea-island structures of bonded polyester branched cores with tangled polyester shell interface areas and unbonded polyester chain areas performed suitable rheological behaviors to recycle polyester textiles for 3D printable filaments production. With the developed polyester textile recycling process and application in the 3D-printing industry, this filament production approach is likely able to alternate landfilling and incineration of polyester textiles, reduce energy and materials use, increase the recycling ratio, reduce the environmental load of textile waste disposal, improve the sustainability of polyester textiles, and promote carbon neutrality. Since the textile wasting is later than its production, the approach in this work can recycle polyester textiles produced by 100% of polyester fibers to deal with the yield boom of single-component polyester textiles in the last decade. To face the industrial development of blended textiles usage and 3D printing material properties enhancement, the approach should be promoted as a bridge to recycling developing textiles for meeting 3D printing material needs.

5 Acknowledgements

The authors would like to express their sincere gratitude to Dr. Sarina Sun, who previously worked at The Hong Kong Polytechnic University, for her invaluable contributions to the conceptualization, methodology design, and discussion of the current work. Her coordination efforts in the cooperation between The Hong Kong Polytechnic University and Jiangsu University were also highly appreciated.

6 References

1. Piribauer B, Bartl AJWM, Research. Textile recycling processes, state of the art and current developments: A mini review. 2019;37(2):112-119.
2. Beton A, Dias D, Farrant L, et al. Environmental improvement potential of textiles (IMPRO-Textiles). *European Commission*. 2014;
3. Wei R, Zimmermann W. Microbial enzymes for the recycling of recalcitrant petroleum-based plastics: how far are we? *Microbial biotechnology*. 2017;10(6):1308-1322.
4. Yoshida S, Hiraga K, Takehana T, et al. A bacterium that degrades and assimilates poly (ethylene terephthalate). *Science*. 2016;351(6278):1196-1199.
5. Zimmermann W, Billig S. Enzymes for the biofunctionalization of poly (ethylene terephthalate). *Biofunctionalization of Polymers and their Applications*. 2011:97-120.
6. Amicarelli V, Bux C. Quantifying textile streams and recycling prospects in Europe by material flow analysis. *Environmental Impact Assessment Review*. 2022;97:106878.
7. Weinmayr G, Pedersen M, Stafoggia M, et al. Particulate matter air pollution components and incidence of cancers of the stomach and the upper aerodigestive tract in the European Study of Cohorts of Air Pollution Effects (ESCAPE). *Environment international*. 2018;120:163-171.
8. Hopewell J, Dvorak R, Kosior E. Plastics recycling: challenges and opportunities. *Philosophical Transactions of the Royal Society B: Biological Sciences*. 2009;364(1526):2115-2126.
9. Kamber NE, Tsujii Y, Keets K, et al. The depolymerization of poly (ethylene terephthalate)(PET) using N-heterocyclic carbenes from ionic liquids. *Journal of Chemical Education*. 2010;87(5):519-521.
10. Raheem AB, Noor ZZ, Hassan A, Abd Hamid MK, Samsudin SA, Sabeen AH. Current developments in chemical recycling of post-consumer polyethylene terephthalate wastes for new

materials production: A review. *Journal of Cleaner Production*. 2019;225:1052-1064. doi:10.1016/j.jclepro.2019.04.019
11. Lang WT, Mehta SA, Thomas MM, Openshaw D, Westgate E, Bagnato G. Chemical recycling of polyethylene terephthalate, an industrial and sustainable opportunity for Northwest of England. *Journal of Environmental Chemical Engineering*. 2023;11(5):110585.
12. Guo Z, Eriksson M, Motte Hdl, Adolfsson E. Circular recycling of polyester textile waste using a sustainable catalyst. *Journal of Cleaner Production*. 2021;283:124579. doi:10.1016/j.jclepro.2020.124579
13. Carr CM, Clarke DJ, Dobson AD. Microbial polyethylene terephthalate hydrolases: current and future perspectives. *Frontiers in Microbiology*. 2020;11:571265.
14. Sadat-Shojai M, Bakhshandeh G-R. Recycling of PVC wastes. *Polymer degradation and stability*. 2011;96(4):404-415.
15. Oblak P, Gonzalez-Gutierrez J, Zupančič B, Aulova A, Emri I. Processability and mechanical properties of extensively recycled high density polyethylene. *Polymer Degradation and stability*. 2015;114:133-145.
16. Schyns ZO, Shaver MP. Mechanical recycling of packaging plastics: A review. *Macromolecular rapid communications*. 2021;42(3):2000415.
17. Li J, Li B, Huang S, et al. Epoxy chain extender grafted pyrophyllite/poly (ethylene terephthalate) composites with enhanced crystallinity and mechanical properties. *Polymer Composites*. 2022;43(9):6404-6415.
18. Saabome SM, Lee JE, Hong JS, Kim DH, Ahn KH. Mechanical degradation of poly (ethylene terephthalate) and its structural modification by chain extender. *Korea-Australia Rheology Journal*. 2023;35(3):203-212.
19. Standau T, Nofar M, Dörr D, Ruckdäschel H, Altstädt V. A review on multifunctional epoxy-based Joncryl® ADR chain extended thermoplastics. *Polymer Reviews*. 2022;62(2):296-350.
20. Wang S, Ma S, Li N, Jie S, Luo Y, Gao X. Branched thermotropic liquid crystal polymer with favourable processability and dielectric properties. *European Polymer Journal*. 2023;196:112302.
21. Wu W-J, Sun X-L, Chen Q, Qian Q. Recycled poly (ethylene terephthalate) from waste textiles with improved thermal and rheological properties by chain extension. *Polymers*. 2022;14(3):510.
22. Hart KR, Frketic JB, Brown JR. Recycling meal-ready-to-eat (MRE) pouches into polymer filament for material extrusion additive manufacturing. *Additive Manufacturing*. 2018;21:536-543. doi:10.1016/j.addma.2018.04.011
23. Maldonado-García B, Pal AK, Misra M, Gregori S, Mohanty AK. Sustainable 3D printed composites from recycled ocean plastics and pyrolyzed soy-hulls: Optimization of printing parameters, performance studies and prototypes development. *Composites Part C: Open Access*. 2021;6doi:10.1016/j.jcomc.2021.100197
24. Mohamed TS, Nassef E, Morsy A, et al. Enhancing 3D printing sustainability: Reinforcing

thermoplastic polyurethane with recycled polyurethane foam for durable applications in orthopedic footwear. *Journal of Vinyl and Additive Technology*. 2024;
25. Tan YA, Chan MY, Koay SC, Ong TK. 3D polymer composite filament development from post-consumer polypropylene and disposable chopstick fillers. *Journal of Vinyl and Additive Technology*. 2023;29(5):909-922.
26. Yap LK, Chun KS, Yeng CM, et al. Effects of corn husk fiber as filler in recycled single-use polypropylene for fused filament fabrication. *Journal of Vinyl and Additive Technology*. 2024;30(2):620-634.
27. Zander NE, Gillan M, Burckhard Z, Gardea F. Recycled polypropylene blends as novel 3D printing materials. *Additive Manufacturing*. 2019;25:122-130. doi:10.1016/j.addma.2018.11.009
28. Zander NE, Gillan M, Lambeth RH. Recycled polyethylene terephthalate as a new FFF feedstock material. *Additive Manufacturing*. 2018;21:174-182. doi:10.1016/j.addma.2018.03.007
29. Singh AK, Bedi R, Kaith BS. Composite materials based on recycled polyethylene terephthalate and their properties – A comprehensive review. *Composites Part B: Engineering*. 2021;219:108928. doi:10.1016/j.compositesb.2021.108928
30. Zhang Y, Ying L, Wang Z, Wang Y, Xu Q, Li C. Unexpected hydrophobic to hydrophilic transition of PET fabric treated in a deep eutectic solvent of choline chloride and oxalic acid. *Polymer*. 2021;234doi:10.1016/j.polymer.2021.124246
31. Oh J, Kim SS, Kim KH, Lee J, Kang C. Structural and physico-chemical properties change of polyethylene terephthalate (PET) fibers after supercritical fluid dyeing with C.I. disperse red 167. *The Journal of Supercritical Fluids*. 2021;170doi:10.1016/j.supflu.2020.105131
32. Ren X, Meng N, Zhang H, et al. Giant energy storage density in PVDF with internal stress engineered polar nanostructures. *Nano Energy*. 2020;72doi:10.1016/j.nanoen.2020.104662
33. Simons WW. *Sadtler handbook of infrared spectra*. Sadtler Research Laboratories; 1978.
34. Nakayama D, Wu F, Mohanty AK, Hirai S, Misra M. Biodegradable Composites Developed from PBAT/PLA Binary Blends and Silk Powder: Compatibilization and Performance Evaluation. *ACS Omega*. Oct 31 2018;3(10):12412-12421. doi:10.1021/acsomega.8b00823
35. Saeb MR, Bakhshandeh E, Khonakdar HA, Mader E, Scheffler C, Heinrich G. Cure kinetics of epoxy nanocomposites affected by MWCNTs functionalization: a review. *ScientificWorldJournal*. Nov 19 2013;2013:703708. doi:10.1155/2013/703708
36. McMurry J. *Organic chemistry*. Ninth edition.. ed. Boston, MA : Cengage Learning; 2016.
37. Park CK, Jang DJ, Lee JH, Kim SH. Toughening of polylactide by in-situ reactive compatibilization with an isosorbide-containing copolyester. *Polymer Testing*. 2021;95doi:10.1016/j.polymertesting.2021.107136
38. Shangguan Y, Zhang C, Xie Y, Chen R, Jin L, Zheng Q. Study on degradation and crosslinking of impact polypropylene copolymer by dynamic rheological measurement. *Polymer*. 2010;51(2):500-506. doi:10.1016/j.polymer.2009.11.066
39. Takeshita H, Shiomi T, Takenaka K, Arai F. Crystallization and higher-order structure of multicomponent polymeric systems. *Polymer*. 2013;54(18):4776-4789.

doi:10.1016/j.polymer.2013.06.031
40. Zhao L, Yu Y, Huang H, et al. High-performance polyphenylene sulfide composites with ultra-high content of glass fiber fabrics. *Composites Part B: Engineering*. 2019;174doi:10.1016/j.compositesb.2019.05.001
41. Samy AA, Golbang A, Harkin-Jones E, Archer E, Tormey D, McIlhagger A. Finite element analysis of residual stress and warpage in a 3D printed semi-crystalline polymer: Effect of ambient temperature and nozzle speed. *Journal of Manufacturing Processes*. 2021;70:389-399. doi:10.1016/j.jmapro.2021.08.054
42. Sakamoto N, Hashimoto T. Ordering Dynamics of a Symmetric Polystyrene-block-polyisoprene. 2. Real-Space Analysis on the Formation of Lamellar Microdomain. *Macromolecules*. 1998/06/01 1998;31(12):3815-3823. doi:10.1021/ma980037s
43. Li L, Aoki Y. Rheological Images of Poly(vinyl chloride) Gels. 1. The Dependence of Sol−Gel Transition on Concentation. *Macromolecules*. 1997/12/01 1997;30(25):7835-7841. doi:10.1021/ma971045w
44. Ji LB, Zhou TR. Finite Element Simulation of Temperature Field in Fused Deposition Modeling. *Advanced Materials Research*. 2010;97-101:2585-2588. doi:10.4028/www.scientific.net/AMR.97-101.2585